Structural characterization of Giardia duodenalis thioredoxin reductase (gTrxR) and computational analysis of its interaction with NBDHEX

GRAPHICAL ABSTRACT

Structural characterization of *Giardia duodenalis* thioredoxin reductase (*g*TrxR) and computational analysis of its interaction with NBDHEX

Simone Brogi, Annarita Fiorillo, Giulia Chemi, Stefania Butini, Marco Lalle, Andrea Ilari, Sandra Gemma, Giuseppe Campiani

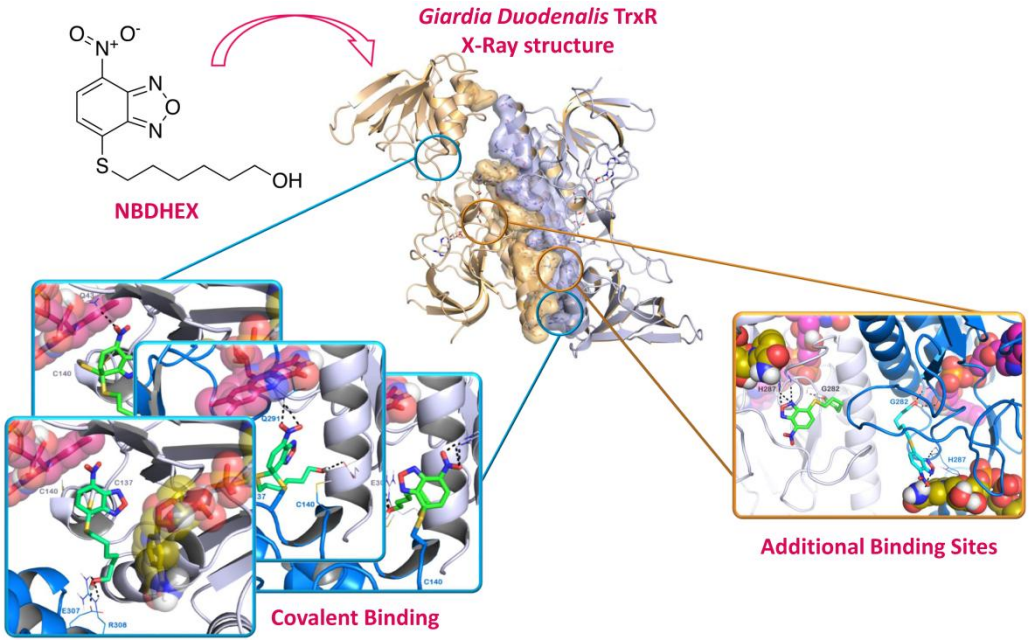

Highlights for the manuscript "**Structural characterization of *Giardia duodenalis* thioredoxin reductase (*g*TrxR) and computational analysis of its interaction with NBDHEX"**

- Crystal structure of *Giardia duodenalis* thioredoxin reductase (*g*TrxR)
- Molecular Modelling of the structure to place cofactors of the enzyme
- Covalent Docking of NBDHEX against *g*TrxR
- Studies regarding the mechanism of inhibition of NBDHEX

Structural characterization of *Giardia duodenalis* thioredoxin reductase (*g*TrxR) and computational analysis of its interaction with NBDHEX

Simone Brogi,[a,1] Annarita Fiorillo,[b,1] Giulia Chemi,[a] Stefania Butini,[a] Marco Lalle[c,*] Andrea Ilari,[b,*] Sandra Gemma,[a,*] Giuseppe Campiani[a]

[a]European Research Centre for Drug Discovery and Development (NatSynDrugs) and Department of Biotechnology, Chemistry, and Pharmacy, Università di Siena via Aldo Moro 2, 53100 Siena, Italy.

[b]CNR (Consiglio Nazionale delle Ricerche) - Istituto di Biologia e Patologia Molecolari (IBPM), c/o Dipartimento di Scienze Biochimiche P.le Aldo Moro 5, 00185, Roma, Italia.

[c]Istituto Superiore di Sanità, Department of Infectious Diseases, viale Regina Elena 299, Rome, Italy.

*Corresponding authors: Sandra Gemma (gemma@unsi.it), Marco Lalle (marco.lalle@iss.it), Andrea Ilari (andrea.ilari@uniroma1.it)

[1]These authors contribute equally to the work

Abstract

Giardia duodenalis is a microaerophilic parasite that colonizes the upper portions of the small intestine of humans. *Giardia* infection is a major contributor to diarrheal disease worldwide. Nitroheterocycles (e.g. metronidazole) or benzimidazoles (e.g. albendazole) are the most commonly used therapeutic agents. Unfortunately, their efficacy is reduced by low compliance or resistance phenomena. We recently discovered that the antitumoral drug 6-(7-nitro-2,1,3-benzoxadiazol-4-ylthio)hexanol (NBDHEX) is active against *G. duodenalis* trophozoites and its mode of action is linked to inhibition of thioredoxin reductase (*g*TrxR), a key component of *Giardia* redox system: *g*TrxR provides efficient defenses against reactive oxygen species (ROS), it is a target of 5-nitroimidazoles antiparasitic drugs and also contributes to their metabolism. However, the exact mechanism responsible for the *g*TrxR inhibition mediated by this chemical class of antigiardial compounds is yet to be defined. The definition of the structural determinants of activity against gTrxR could be important for the identification of novel drugs endowed with an innovative mode of action. With this aim, we solved the crystal structure of *g*TrxR and we analyzed *in silico* the binding mode of NBDHEX. The data presented herein could guide the development of NBDHEX derivatives tailored for selective inhibition of *g*TrxR as antigiardial agents.

Keywords: *Giardia duodenalis*, crystal structure of thioredoxin reductase (*g*TrxR), NBDHEX, protein modeling, covalent docking

1. Introduction

Giardia duodenalis (syn. G. lamblia, G. intestinalis) is a cosmopolitan protozoan parasite that colonizes the upper portions of the small intestine of mammals, being responsible in humans of giardiasis, one of the most commonly reported protozoan intestinal infection [1]. Giardiasis is a neglected tropical disease (NTD) and has been included in the "Neglected Diseases Initiative" in 2004 [2]. *G. duodenalis* treatment mostly relies upon the nitrohetorocyclic class of drugs represented by metronidazole (MTZ, Figure 1) or the benzimidazoles class represented by albendazole (ALB, Figure 1) [3]. However, treatment failure (especially with MTZ) has been reported due to several factors including non-compliance to the therapy, immune deficiency or drug resistance. So, the development of optimized and efficacious therapies represents an unmet medical need and optimized therapies and novel antigiardial compounds are highly needed [4].

Recently we have shown that the 6-(7-nitro-2,1,3-benzoxadiazol-4-ylthio)hexanol (NBDHEX, Figure 1), a glutathione S-transferase non-peptide inhibitor and a promising antitumoral compound, is toxic for *G. duodenalis* trophozoites at concentration (μM) lower than MTZ [5]. We then engaged in the investigation of NBDHEX targets in order to better clarify its mode of action. We showed that NBDHEX administration to *G. duodenalis* trophozoites results in a significant reduction of the parasite FAD-dependent glycerol-3-phosphate dehydrogenase (gG3PD) [5] activity and that this compound also tightly binds thioredoxin reductase (*g*TrxR) [6]. Upon *g*TrxR binding, NBDHEX concomitantly inhibits the NADPH-dependent disulphide reductase activity and promote NADPH oxidase activity of the enzyme in a dose-dependent manner [6]. Administration of NBDHEX to parasite cells and *in vitro* to recombinant *g*TrxR in presence of NADPH, led to the formation of covalent adducts with the catalytic cysteines (Cys137 and Cys140) and nitro-reduced form of the drug. Moreover, the NBDHEX is modified by *g*TrxR *in vitro*, likely by nitroreduction [6].

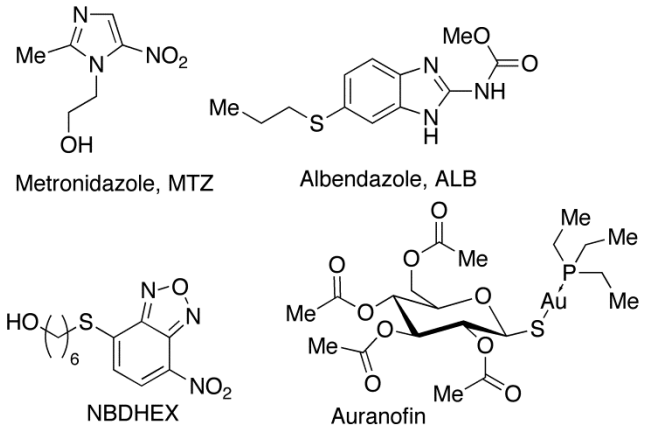

Figure 1. Chemical structures of MTZ, ALB, NBDHEX and auranofin.

Interaction of NBDHEX with *g*TrxR is highly interesting due to the specific redox metabolism of *Giardia*. Although inhabiting fairly aerobic environments, *G*. *duodenalis*, like other miroaerophilic parasites, requires efficient defenses against reactive oxygen species (ROS), produced either by its own metabolic processes or by the host defense mechanisms. *G*. *duodenalis*, like *T*. *vaginalis* and *E*. *hystolitica*, is devoid of the conventional enzymes responsible for antioxidant defense, such as superoxide dismutase, catalase and glutathione cycling [7, 8]. Scavenging of hydroxyl radicals is accomplished by cysteine, non-protein thiols and pyruvate, whereas protein thiols are kept in their functionally reduced state by the thioredoxin (Trx)-TrxR system [9, 10].

TrxR, along with other components of the redox system, has also been implicated in the metabolism of antiparasitic drugs. 5-Nitroimidazoles antigiardial drugs, such as MTZ, become toxic when their nitro moiety is reduced to the highly reactive nitroradical anion (or further reduced nitrosoimidazole or hydroxylamineimidazole intermediates) that impairs cell functions reacting with nucleic acid and proteins [11, 12]. TrxR and Ferredoxin (Fd)/pyruvate:ferrodoxin oxidoreductase (PFOR) are responsible of 5-nitroimidazoles reduction in *G*. *duodenalis*, *T*. *vaginalis* and *E*. *hystolitica* [13-18]. Auranofin (Figure 1), a gold salt approved by FDA for treatment of rheumatoid arthritis, is also active against *E*. *hystolitica* and *G*. *duodenalis* and is reported to semicompetitively inhibit *E*. *hystolitica* TrxR, and likely also the *G*. *duodenalis* enzyme [19, 20]. Although the structure of *Eh*TrxR in presence of auranofin has been solved, the mechanism of TrxR inhibition is far to be clarified. In fact, no Au(I) was found to bind in the active site to eventually prevent electron transfer

from TrxR and its substrate [21]. Overexpression of *g*TrxR in *G. duodenalis* indeed increases the susceptibility to 5-nitrocompounds (i.e. MTZ and furazolidone) but has no effect when parasite is treated with ALB, auranofin or the nitrothiazolide nitazoxanide [22]. Although only auranofin proved to reduce disulphide reductase activity of TrxR *in vitro*, *G. duodenalis* *g*TrxR seems to not be a key target of any drug presently used for the treatment of giardiasis [23].

TrxRs are NADPH-dependent flavin enzymes belonging to the nucleotide disulfide oxidoreductase family. They function as homodimers with each monomer possessing a FAD prosthetic group, a NADPH binding site and an active site comprising a redox-active disulfide [24, 25]. TrxR catalyzes the disulfide reduction of oxidized Trx via FAD and the redox-active cysteines using NADPH as reductant. Two classes of TrxRs are known: i) the high molecular weight (~55kDa, H-TrxRs), present in higher eukaryotes and in protozoan parasites of the phylum Apicomplexa, and ii) the low molecular weight (~35 kDa, L-TrxRs), found in archaea, bacteria, plants, and lower eukaryotes. *G. duodenalis* harbors a constitutively expressed single L-TrxR of approximately 33.8 kDa (*g*TrxR, *GiardiaDB*) [26]. The structures of several L-TrxRs have been solved [21, 27-31] showing that the catalytic cycle of L-TrxR requires a large conformational change of one domain. L-TrxRs display two different conformations. The flavin-reducing conformation (FR), allowing flavin reduction by NADPH, and the flavin-oxidizing conformation so called (FO) allowing the reduction of the disulfide loop of the enzyme by FAD [32]. Transition between the two conformations implies a rotation of the NADPH domain of ~ 67° around an axis perpendicular to the interface between the FAD and the NADPH binding domains [28, 32]. In the FO structures, the enzyme displays a closed conformation (CC) where the dithiol-disulfide redox centers are close to the *re face* of the flavin and displays an orientation that allows the reduction of the disulfide bond with concomitant oxidation of the flavin. In FR conformation the reduced cysteine residues (Cys135 and Cys138 in *E. coli* TrxR) are placed on the external surface of the NADPH binding domain allowing the reduction of Trx whereas the nicotinic ring of NADPH forms a stacking interaction with the FAD isolalloxazine ring [32].

In order to gain some insight into the mechanism governing the inhibitory activity of NBDHEX

against *g*TrxR, the crystallographic structure of *g*TrxR in its apo form was determined and used for computational experiments aimed at analyzing the structural interactions of NBDHEX with *g*TrxR. We performed our *in silico* analysis by applying an extensive computational protocol, consisting of i. *g*TrxR protein modeling (building missing side-chains, loop refinement, localization of cofactors, protein minimization), ii. molecular docking simulation for providing the binding mode of NBDHEX upon reaction with cysteine residues (covalent docking, ligand binding energies estimation) and iii. prediction and analysis of other potential binding sites. The computational analysis highlighted the potential mechanism and the favorable position of NBDHEX for the covalent attack of cysteine reactive residues. Given the activity of NBDHEX against *G*. *duodenalis* trophozoites and the role of *g*TrxR in their redox metabolism, the identification and analysis of the binding site of NBDHEX within *g*TrxR could furnish important clues in order to design optimized analogues.

2. Materials and Methods

2.1. Expression and purification of the recombinant protein

The full-length coding sequence of TrxR from the isolate WB-C6 of *Giardia duodenalis* (*g*TrxR, GL50803_9827) was cloned and expressed as N-terminal 6XHIS tagged protein in *E. coli* M15 strain as previously reported [6]. HIS-*g*TrxR was affinity purified on native condition on Ni-NTA Agarose (Qiagen, Germany) and eluted with 250 mM imidazole according to the manufacturer. Purified protein (purity ≥ 95%) was dialyzed against 20 mM Hepes, 10 mM NaCl at pH 7.0 at a final concentration of 10 mg/mL.

2.2. Protein crystallization, data collection and data reduction

The protein was crystallized at 298 K by the hanging-drop vapor diffusion method. Aliquots (1.0 μL) of the protein sample were mixed with an equal amount of reservoir solution containing bis tris buffer 0.1 M pH=6.5 and PER-MME 20 % w/v and were allowed to equilibrate with a 500 μL volume of reservoir solution. Crystals grew in one week and reached dimensions of 0.05 × 0.05 × 0.3 mm. 6XHIS-*g*TrxR crystals were mounted in nylon loops and flash frozen by quick submersion into liquid nitrogen for transport to the synchrotron-radiation source. A single-wavelength data set (λ = 0.918 Å) was collected from a single HIS-*g*TrxR crystal at the BL-14.1 beamline of the Synchrotron Radiation Source BESSY (Berlin, Germany), using a Pixel detector DECTRIS-PILATUS 6M-F at a temperature of 100 K. The data processed with XDS [33] indicate that the crystal belongs to the $P4_12_12$ space group and its unit cell displays the following dimensions: a=b=85.643 Å, c=163.221 Å. Crystal parameters and data collection statistics for the measured crystal are listed in Table 1.

2.3. Structure solution and refinement

The structure of HIS-*g*TrxR was determined by molecular replacement using *Sc*TrxR structure (PDB code 3D8X) as search model. The rotational and translational searches performed with the program MOLREP [34], CCP4 suite, in the resolution range 10.0 – 3.0 Å produced a clear solution,

corresponding to a dimer in the asymmetric unit. Refinement was performed using the maximum-likelihood method with the program REFMAC [35] while the Coot program [36] was employed for model building (see Table 1). The quality of the model was assessed using the program PROCHECK [37]; all the residues of the structure were within the allowed or generously allowed regions of the Ramachandran plot (see Table 1). The structure was refined to 2.65 Å resolution. The final R_{crys} value was 20.5 %, and the R_{free} one was 26 %.

The final model contains two monomers (A and B) monomer A (residues 4-312), monomer B (residues 3-314) two FAD molecules, 49 water molecules, one sodium ion.

The coordinates have been deposited in the Protein Data Bank with the PDB code 5M5J.

Table 1. Crystal parameters, data collection statistics and refinement statistics of *g*TrxR

PDB code	5M5J
Space group	$P4_12_12$
Unit cell parameters (Å)	
a	85.64
b	85.64
c	163.22
No. of molecules in the asymmetric unit	2
$\langle B \rangle$ for atomic model (Å^2)	45
Data analysis ranges (highest resolution shell) (Å)	48.6–2.65(2.65-2.78)
Unique reflections	18404
Completeness (%)	99.8 (99.2)
Redundancy	16(15.3)
[a]Rmerge	0.27(1.46)
CC(1/2)	0.99(0.77)
$\langle I/\sigma(I) \rangle$	12.1(2.2)
Refinement ranges (highest resolution bin)	48.6-2.65(2.65-2.72)
R_{crys} (%)	20.2 (28.6)
R_{free} (%)	26.0 (31.1)
rms (angles) (°)	1.258
rms (bonds) (Å)	0.008
Residues in core region of Ramachandran plot (%)	98
Residues in generously allowed region of Ramachandran plot (%)	2

Values in parentheses are for the highest-resolution shell.

[a] $R_{merge} = \sum_{hkl}\sum_i |I_i(hkl) - \langle I(hkl) \rangle| / \sum_{hkl}\sum_i I_i(hkl)$, where $I_i(hkl)$ is the *i*th observation of the reflection (*hkl*) and $\langle I(hkl) \rangle$ is the mean intensity of the (*hkl*) reflection.

2.4. Computational details

2.4.1. Protein refinement and preparation

The crystal structure of *g*TrxR was firstly submitted to an extensive refinement protocol in order to add the missing side-chains of the original crystal structure. In particular, the chain B of the crystallized dimeric form of *g*TrxR was imported into Prime software (Prime, version 3.9, Schrödinger, LLC, Release 2015) implemented in Maestro suite (Maestro. version 10.1, Schrödinger, LLC, Release 2015) in order to re-built the missing parts of the protein. The resulting structure was then used to replace the existent chain B of the crystal structure. The obtained dimer of *g*TrxR was then used to place the NADPH cofactor in both chains.

For the chain A of *g*TrxR in CC, NADPH cofactor was extracted from 1TDF (TrxR from *E. coli*) and placed in the appropriate binding site after the superposition of the two proteins. The binding site of *g*TrxR, due to its high degree of conservation, was modelled according to the 1TDF (both chains, chain A from *g*TrxR crystal structure and chain A from 1TDF, were perfectly superposed due to their similar CC).

For the chain B of *g*TrxR, since the open conformation (OC) of the protein has not crystallized thioredoxin reductase homologues in the same form, we adopted an induced fit docking protocol to accommodate the NADPH in the open chain B (see Induced Fit Docking paragraph).

The resulting three-dimensional structure of *g*TrxR was imported into Maestro suite 2015 and submitted to protein preparation wizard to obtain a reasonable starting structure for docking calculation.

2.4.2. Induced Fit Docking (IFD)

Molecular docking to accommodate NADPH cofactor into chain B of *g*TrxR was carried out using the Schrödinger suite 2015 by applying the IFD protocol [38-41] (Induced Fit Docking protocol 2015; Glide version 6.4, Prime version 3.7, Schrödinger, Release 2015). This procedure induces conformational changes in the binding site to accommodate the ligand and exhaustively identify possible binding modes and associated conformational changes by side-chain sampling and

backbone minimization. The protein (chain B) was prepared as reported in the previous paragraph. The box for docking calculation was built taking into account the centroid of the conserved arginine residues (119, 178, 179, 183, and 290) with default setting. IFD includes protein side-chain flexibility in a radius of 5.0 Å around the poses generated during the initial docking step of the IFD protocol. Complexes within 30.0 kcal/mol of minimum energy structure were taken forward for redocking. The Glide redocking stage was performed by means of XP (Extra Precision) methods. The calculations were performed employing default IFD protocol parameters. No hydrogen bonding or other constraints were adopted.

The resulting model of *g*TrxR in complex with NADPH was submitted to a refinement protocol as previously reported by us [42-46] by means of Prime software. The protocol consists of side-chains optimization and loops refinement for the rebuilding regions. Further structure optimization was performed on the whole protein by means of MacroModel (MacroModel, version 10.7, Schrödinger, LLC, Release 2015) software implemented in Maestro suite 2015 using the OPLS-2005 as force field with 10,000 maximum iterations and 0.001 as convergence threshold using PRCG method [47, 48]. During this calculation the NADPH binding site in chain B was minimized taking into account the conserved contacts with arginine residues 119, 178, 179, 183, and 290. The refined model in comparison with the crystal structure is reported in Figure 2.

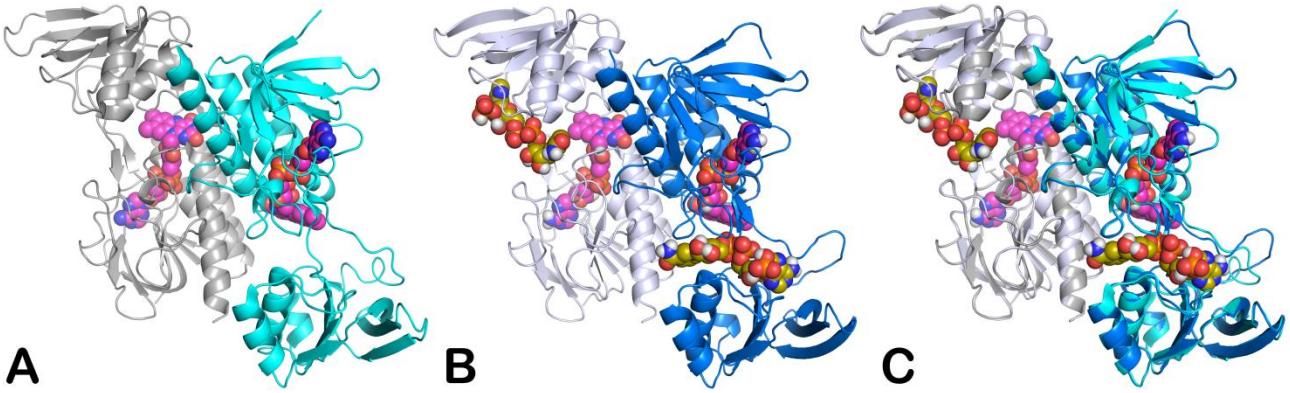

Figure 2. (A) Crystal structure of *g*TrxR (chain A in grey and chain B in cyan); **(B)** refined model of *g*TrxR (chain A in light grey and chain B in blue); **(C)** Superposition between the crystal structure and the refined model of *g*TrxR. FAD cofactor is represented by magenta spheres, while the added NADPH cofactor is represented in spheres and coloured in dark yellow. The pictures were generated by means of PyMOL (The PyMOL Molecular Graphics System, v1.7.2.1;

Schrödinger, LLC, New York, 2015).

The quality of the obtained *g*TrxR model was evaluated by RAMPAGE (http://mordred.bioc.cam.ac.uk/~rapper/rampage.php access date December 2016). The result of RAMPAGE webserver revealed that over 99% of the residues (597 residues, 96.4% in favoured region; 22 residues, 3.6% in allowed region and 0% of residues in outlier region) of our *g*TrxR refined model sit in the allowed regions of Ramachandran Plot (Figure S1). This value is higher than the cut-off value (96.1%) defined for the most reliable models [49, 50]. Consequently, the stereo-chemical quality of our model was acceptable, displaying no residues in outlier regions.

2.4.3. Covalent Docking

Covalent docking studies were performed in Maestro suite 2015 adopting the Covalent Docking protocol (CovDock) [51]. The algorithm utilizes both Glide (Glide, version 6.6, Schrödinger, LLC, Release 2015) and Prime (Prime, version 3.9, Schrödinger, LLC, Release 2015) software. CovDock considers custom reactions that are present in a list of possible covalent reactions (implemented in the software) using SMARTS pattern, so it is possible to automatically recognize the reactive residue and the portion of the ligand that are involved in the reaction. If the desired reaction is not present in that list, it is possible to write the reaction that involves the correct atoms. In this study, since the desired reactions were not present in the list of reactions provided by CovDock, the reaction SMARTS pattern was customized in order to obtain a reliable reaction for the NBDHEX. Once the correct reaction is written and the software recognizes all the residues involved, CovDock initially combines the Glide docking algorithm and Prime structure refinement, for determining if the ligand can accommodate into the selected binding site (standard docking). In this way, the ligand should be located in a suitable position close to the reactive group of the reactive residue, as a constraint. The reactive residue, cysteine or serine, is mutated with an alanine residue, for generating an initial association in which the ligand is non-covalently bound to the receptor. After that, the receptor is restored and the reaction occurs. Once the covalent bond is formed the complex

is minimized. Now the obtained poses are clustered and ranked after a complete minimization.

Concerning NBDHEX positions C4 and C6 of the nitrobenzofurazan could be suitable for nucleophilic attack of reactive cysteine residues as previously reported (see Results and Discussion for a comprehensive view) [52].

Accordingly, two reaction types were created and two files were generated: for the position C6 (C6.cdock), and for the position C4 (C4.cdock) (see Table S1 in the Supplementary Material for further details). In the .cdock files the settings specify the reactive atoms of the considered cysteine residues (Cys137 and Cys140) and of the ligand taking into account the two different positions for the reaction. So, the calculation output consists in eight covalent docking complexes to further evaluate (four for each chain).

To start the calculation, the reactive residues of the receptor were selected in both chains (Cys137 and Cys140 respectively), and matched to the ones defined in the custom chemistry file. The grid center was positioned at the centroid of the selected residue, and the size of the grid box was automatically determined. After the ligand selection, the option Custom was chosen from the Reaction Type tab and the custom .cdock file uploaded. No constraints were chosen and a Pose Prediction protocol was chosen in order to obtain more accurate output results. Following the docking procedure, the obtained poses are filtered and for the Refinement step all the default parameters were retained. The scoring option MM-GBSA was selected in order to obtain more information about the binding affinity of the poses. NBDHEX as the ligand and the refined *g*TrxR protein were used for the covalent docking procedure. In particular, NBDHEX was built in Maestro and then prepared by LigPrep (LigPrep, version 3.3, Schrödinger, LLC, Release 2015) application at cellular pH to avoid any potential error in drawn structure. Regarding the refined *g*TrxR (chain A and B) the disulfide bonds between Cys137 and Cys140 were manually broken and the loops containing the reactive cysteine residues were minimized (by Prime loop refinement module) taking into account the structure of TrxR of *E*. *Coli* (PDB code 1TDF) in which the disulfide bond is not present. For each chain a covalent docking calculation was performed on both cysteine residues since experimental data did not allowed to ascertain which of the two residues are involved in the

reaction. Covalent docking of MTZ was performed as described above considering the C4 position of MTZ as the attack position of both cysteine residues for each chain of *g*TrxR [17]. Accordingly, a reaction type was created and one file was generated for the position C4 (MTZC4.cdock) (see Table S1 in the Supplementary Material for further details). In the .cdock files the settings specify the reactive atoms of the considered cysteine residues (Cys137 and Cys140) and of the ligand taking into account the position for the reaction. So, the calculation output consists of four covalent docking complexes to further evaluate (two for each chain).

2.4.4. Estimated ligand binding energies

The Prime/MM-GBSA method implemented in Prime software was used to score the docked poses for both covalent and non-covalent complexes. The calculations consist in computing the change between the free and the complex state of both the ligand and the protein after energy minimization. Regarding the covalent docking output the binding affinity was calculated on the non-covalent binding of the capped final pose to the mutated receptor as specified in CovDock user manual. For the non-covalent docking complexes herein reported, the calculation was performed as previously reported [53-56].

2.4.5. Binding sites prediction and non-covalent docking

Sitemap (SiteMap, version 3.4, Schrödinger, LLC, Release 2015) was used to predict the potential binding sites of *g*TrxR with the default settings introducing ten as maximum number of reported binding sites. Non-covalent docking calculations were performed by Glide (Grid-Based Ligand Docking with Energetics) (Glide, version 6.6, Schrödinger, LLC, Release 2015) using NBDHEX and *g*TrxR prepared as described above, applying Glide extra precision (XP) method. Energy grids were prepared using default value of protein atom scaling factor (1.0 Å) within a cubic box centered on the residues comprised in the predicted binding sites calculated by SiteMap. The number of poses entered to post-docking minimization was set to 10. Glide XP score was evaluated. The main contacts of NBDHEX with *g*TrxR were evaluated by means of ligand-interaction diagram coupled

to a script for displaying hydrophobic interactions implemented in Maestro 2015.

3. Results and Discussion

3.1. Structural analysis: *g*TrxR overall fold

The structure of *g*TrxR has been solved by molecular replacement with the program Molrep using as template the structure of cytosolic thioredoxin reductase-1 from *Saccaromices cerevisiae* (*Sc*TrxR1, PDB code 3D8X) as search model. The *Sc*TrxR shares 45% sequence identity (144/320 residues) with *g*TrxR (Figure 3). The crystal contains a dimer in the asymmetric unit (monomers A and B in Figure 4). In both monomers in the absence of NADPH, the redox-active disulfide (Cys137-Cys140) was in its oxidized form.

The models contain 620 residues (model A residues 4-312; model B residues 3-314), however, in the model B the residues 119-132 are not clearly visible in the structure.

Similarly to the other structures solved so far (*S*. *cerevisiae*, *E*. *hystolitica*, Archaea, bacteria, and plant) [21, 27-31], the *g*TrxR monomer is composed of two typical Rossman folds (β-α-β-α-β domains) that form the binding sites of NADPH and FAD, respectively (Figure 4). The FAD binding domain is composed of residues 1-118 (β strands 1-8 and α helices 1-3) and 241-312 (β strand 15 and α helices 9-11) whereas the NADPH binding domain is composed by the residues 119-240.

Figure 3. Structural alignment of *g*TrxR with *S*. *cerevisiae* TrxR, *E*. *coli* TrxR and *E*. *histolitica* TrxR. The secondary structure elements are indicated.

The monomers A and B display different conformations. Indeed, the Cα alignment of the two monomers A and B performed with the program COOT (SSM algorithm) yields a RMSD of 2.82 Å (number of aligned residues: 267). The high value RMSD indicates that the two monomers display different conformations and are not superimposable, as clearly evident by superimposing only the residues of the FAD binding domain of the two monomers (Figure 4). In particular, the monomer A displays a conformation identical to that described for *E*. *coli* TrxR [32] named FO. In this conformation, the disulfide loop of the enzyme is close to the *re* face of the flavin but distant from

the NADPH binding site and buried in a position where they cannot react with the substrate.

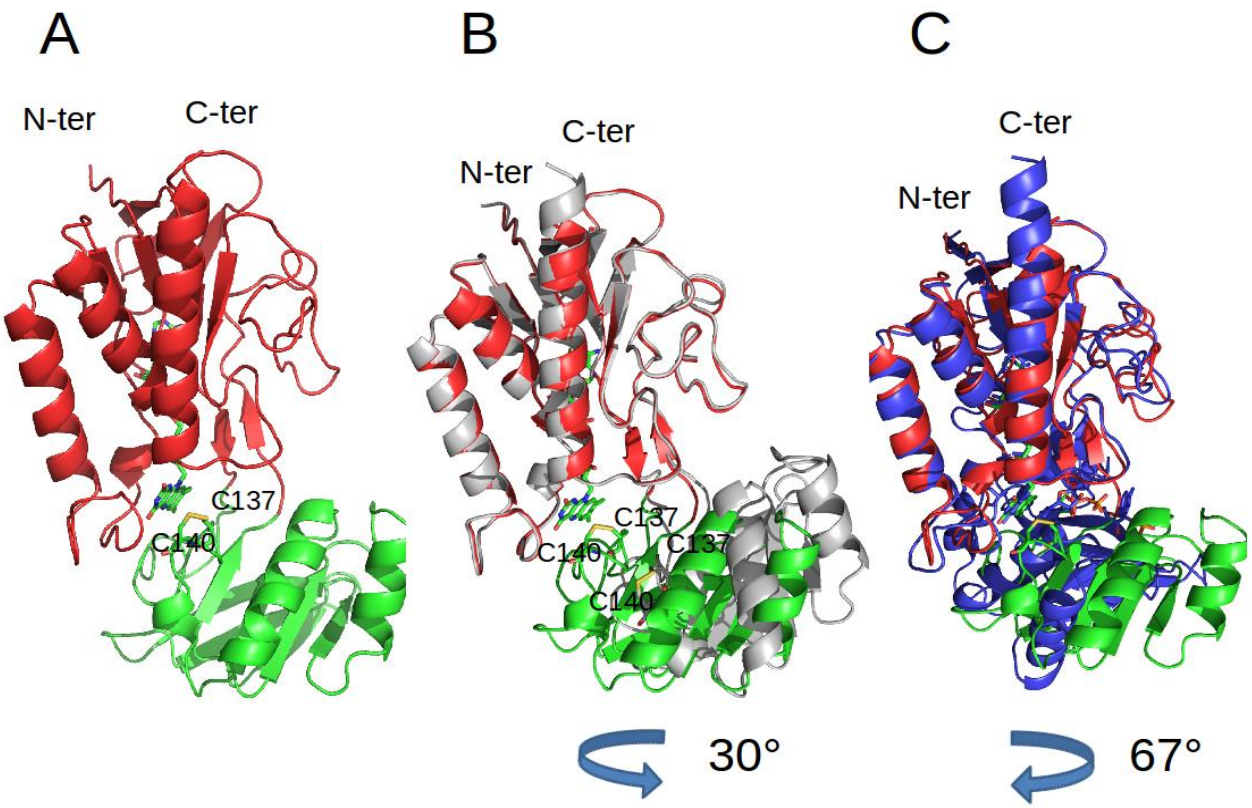

Figure 4. **(A)** Ribbon representation of the monomer A. The FAD binding domain is colored red and the NADPH binding domain is colored green. The FAD molecule and the two catalytic cysteines (C137 and C140) are depicted as sticks and colored green. **(B)** Superimposition between the monomers A and B. The monomer B is colored grey. The FAD coenzyme and the two catalytic cysteines forming a disulfide bridge are represented as sticks. (**C**) Superimposition between the *Ec*TrxR in FR conformation (colored blue) (PDB code 1F6M) and the monomer A of *g*TrxR.

The superimposition of monomer A of *g*TrxR with monomer A of the *S*. *cerevisiae* TrxR yields a RMSD of 0.825 with 259 residues structurally aligned, indicating similarity between the structures. On the contrary, the RMSD of the superimposition between monomer B and monomers A-C of *S*. *cerevisiae* TrxR (PDB code 3ITJ) ranges from 2.23 and 2.94 Å indicating that the *g*TrxR monomer B does not adopt the FO conformation. Indeed, following superimposition of FAD binding domains of the two *g*TrxR monomers (Figure 4B), the NADPH binding domain shows a rotation of about -30° with respect to the FAD binding domain, adopting an anticlockwise open conformation (AOC)

where the two catalytic cysteines are far away from the FAD molecule. This conformation (Figure 4C) differs also from the FR conformation described for *E. coli* TrxR [32], where a clockwise open conformation allows the TrxR interaction with thioredoxin. In the conversion of *E. coli* TrxR from FO to the FR conformation, the NADPH domain rotates 67° about the axis passing through the two domains (clockwise) [32]. Instead, in the solved *g*TrxR structure the conformational change from monomer A to monomer B conformation implies a rotation of -30° about the same axis (anticlockwise).

3.2. Interfaces analysis

The analysis of the solvent accessible surface area (SASA), which has been performed using the program face2face (http://apps.ibpm.cnr.it/f2f/index), shows that the buried area at the dimeric interface decreases in *g*TrxR with respect to both the *Ec*TrxR in FR conformation (PDB code 1F6M) and the *Sc*TrxR in FO conformation. In particular in *g*TrxR the polar interactions between the two monomers strongly decrease with respect to both the FO and FR conformations (Figure 5, Table 2).

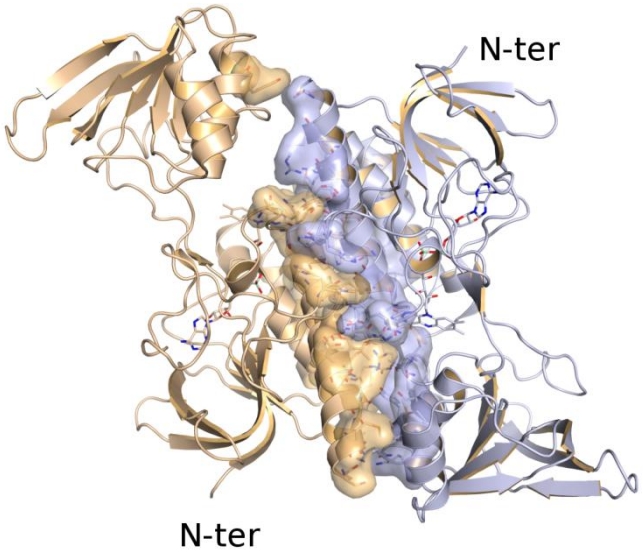

Figure 5. Surface of interaction between the monomers A (colored in salmon) and B (colored in cyan).

Table 2. Comparison of the SASA accessible area in *g*TrxR, *Ec*TrxR in FR conformation and *Sc*TrxR in FO conformation.

Dimeric Interface	*g*TrxR	FR (1F6M)	FO (3ITJ)
Buried Area Complex (Å^2)	4061.8	4369.9	4226.2
Buried Area Complex (%)	13.6	13.8	14.1
Surface Area (Å^2)	2030.9	2184.95	2113.1
Interface Area CHAIN B (%)	13.3	13.8	14.1
Interface Area CHAIN A (%)	13.9	13.7	14.0
APOLAR Interface (Å^2)	2693.0	2722.4	2624.3
APOLAR Interface (%)	66.3	62.3	62.1
APOLAR Interface Area (Å^2)	1346.5	1361.2	1312.15
POLAR Interface (Å^2)	1368.7	1647.4	1602.1
POLAR Interface (%)	33.7	37.7	37.9
POLAR Interface Area (Å^2)	684.35	823.7	801.05
Residues at the interface TOT(n)	102	118	106
Residues at the interface CHAIN B	54	59	56
Residues at the interface CHAIN A	48	59	50

As shown for *Ec*TrxR, in the conversion from the FO to the FR conformation, contacts between the NADPH domain and each of the two FAD domains of the dimer break and new contacts are formed [32]. Most of the same residues from the NADPH domain contribute to both interfaces, but they contact different regions of the FAD domains. The interface between the NADPH and FAD domains decreases in area from about 1000 Å^2 in FO to 630 Å^2 in FR, exposing the catalytic cysteines in the NADPH domain for interaction with thioredoxin [32].

In the *g*TrxR structure we have the unique opportunity to compare monomer A with a conformation identical to the FO conformation of *Ec*TrxR that we will call closed conformation (CC) and monomer B which display an anticlockwise open conformation (AOC) with the FAD isolalloxazine ring exposed to the solvent. As for the conversion from the FO to the FR conformation, the conversion from the CC to the AOC implies a decrease in the interface area between the two domains that moves from 1296.5 Å^2 to 714.2 Å^2. In particular, the apolar interface decreases from 716.2 in the CC to 460.7 Å^2 in AOC and the polar interface decreases from 580.2 Å^2 in CC to 253.6 Å^2 AOC (Figure 6, Table 3).

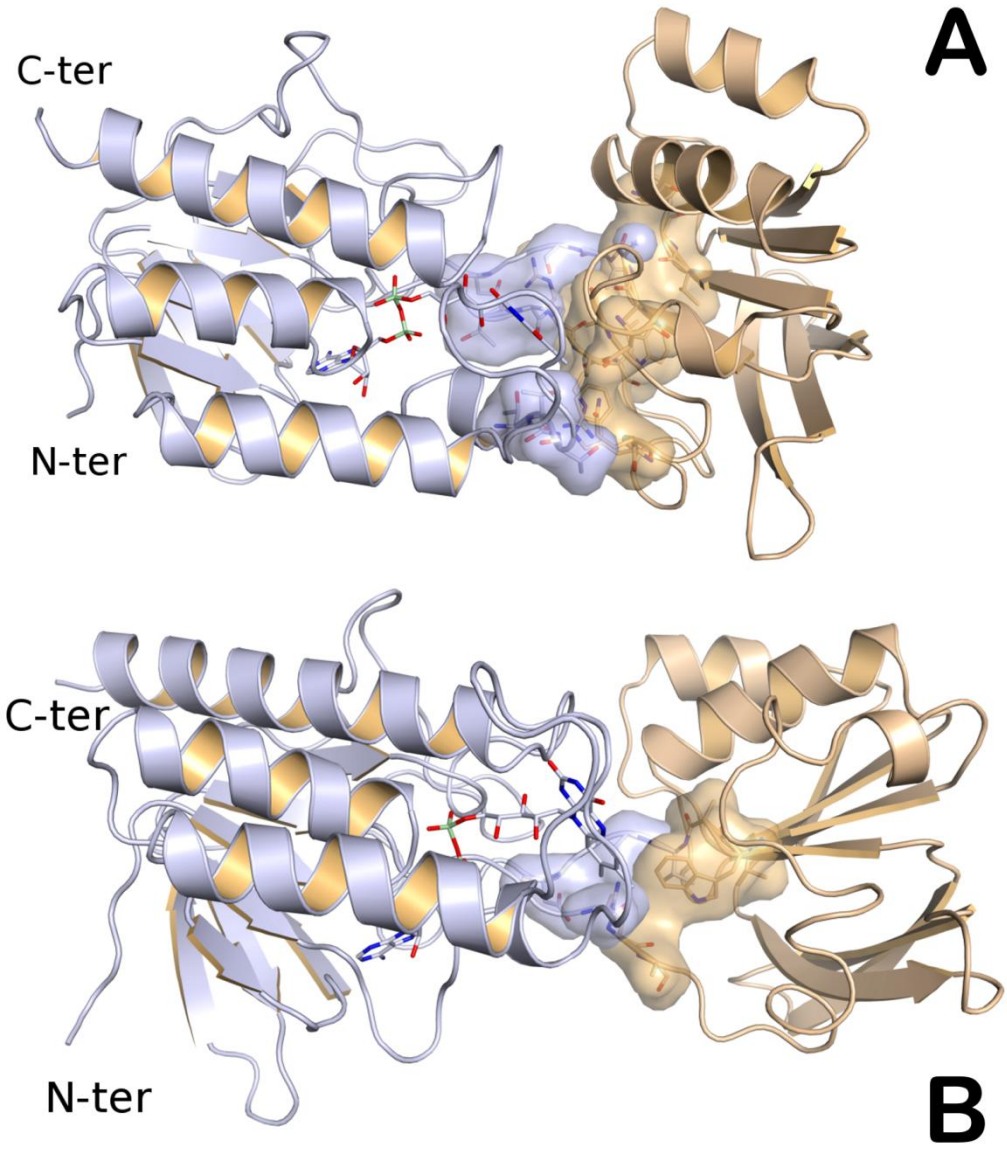

Figure 6. Area of interface between the FAD binding domain and NADPH binding domain. (**A**). Area of interface in the monomer A; (**B**). Area of interface in the monomer B.

Table 3. Comparison of the SASA accessible area between the NADPH binding domain and FAD binding domain in MonA and MonB.

Interface between the NADPH and FAD binding domains	Mon A (CC)	Mon B (OC)
Buried Area Complex (Å^2)	1296.5	714.2
Buried Area Complex (%)	8.1	4.5
Surface Area (Å^2)	648.25	357.1
Interface Area NADPH binding domain (%)	6.8	3.7
Interface Area FAD binding domain (%)	10.1	5.6
APOLAR Interface (Å^2)	716.2	460.7
APOLAR Interface (%)	55.2	64.5

APOLAR Interface Area (Å^2)	358.1	230.35
POLAR Interface (Å^2)	580.2	253.6
POLAR Interface (%)	44.8	35.5
POLAR Interface Area (Å^2)	290.1	126.8
Residues at the interface TOT(n)	40	24
Residues at the interface NADPH binding domain	18	12
Residues at the interface FAD binding domain	22	12

3.3. Interaction of NBDHEX with *g*TrxR

Despite several attempts, we were unable to obtain diffraction quality crystals of *g*TrxR in complex with NADPH and/or NBDHEX. Consequently, we applied bioinformatics analyses to investigate the inhibitory mechanism of NBDHEX against *g*TrxR. We first analyzed the reactions reported in Figure 7 [52]. Experimental evidences suggest that NBDHEX can tightly bind to *g*TrxR in its oxidized fluorescent form, also in the absence of NADPH, likely by cysteine attack at two different drug positions (C4 and C6) of the bicyclic system. We also observed that the binding and enzyme inhibition follows a biphasic behavior [6]. Adducts between the nitro-reduced form of the drug and, mainly, the catalytic Cys137 and Cys140 of *g*TrxR could be detected by mass spectrometry analysis but only when NADPH was present [6]. This would suggest that both Cys137 and Cys140 could react with NBDHEX. With the nitro-group in place, NBDHEX is an excellent electrophile and rapidly forms σ-complexes with nucleophiles such as the sulphur atoms of the cysteine residues that can attack both C4 or C6 positions [52, 57].

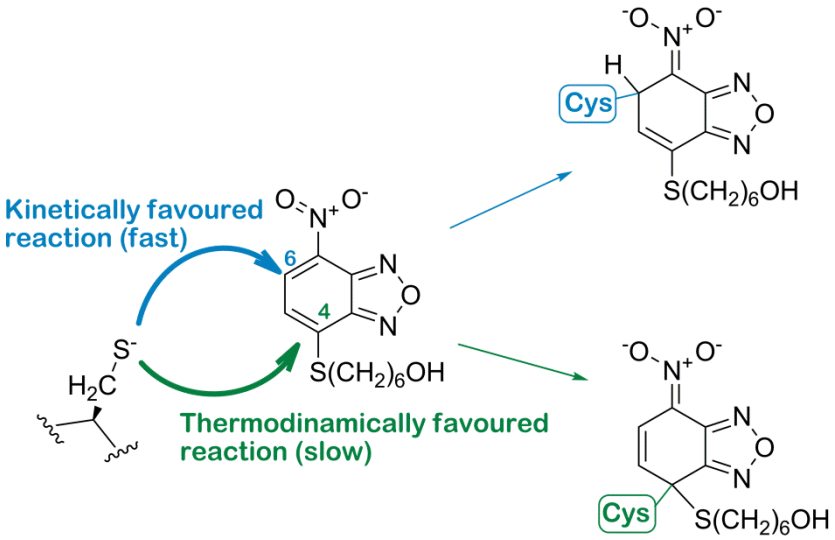

Figure 7. Schematic representation of the reactions occurring among the different positions of NBDHEX and the Cys137 and Cys140 residues of *g*TrxR.

Based on experimental observations and the peculiar conformation of each monomer of the solved *g*TrxR dimer, docking calculations were performed using both chains of the dimeric structure of *g*TrxR and NBDHEX with its C4 and C6 positions for the attack of Cys137 and Cys140. By using the mentioned procedure with the protein and the ligand prepared as reported in the Materials and Methods section, GlideScore and ligand binding energy (ΔG_{bind}) values for each complex were calculated (Table 4). GlideScore and ΔG_{bind} of the covalent docking complexes measure the affinity of the ligand to the receptor for non-covalent binding prior to reaction. Ligands with a not favorable score are considered less likely to approach the receptor in a way that allows covalent bond formation. To calculate the score, the bond is broken again, the reactive receptor residue is mutated to alanine, and the bond to the ligand is capped with hydrogen. Scoring is then done in place with Glide, and the affinity is reported as the average of the pre-reacted and post-reacted GlideScore for a given pose (CovDock user Manual, Schrödinger Press, LLC, New York, Release 2015).

Table 4. Computational data for the NBDHEX binding both chains of *g*TrxR as found by covalent docking protocol.

	***g*TrxR-chain A**				***g*TrxR-chain B**			
	Cys137		**Cys140**		**Cys137**		**Cys140**	
NBDHEX	GlideScore	ΔG_{bind}	GlideScore	ΔG_{bind}	GlideScore	ΔG_{bind}	GlideScore	ΔG_{bind}
Position 4	-5.89	-34.19	-4.43	-37.72	-4.07	-36.35	-4.37	-42.05
Position 6	-5.57	-28.18	-4.56	-29.23	-4.03	-29.71	-3.97	-31.01

As reported in Table 4, the covalent bond can indeed occur for both Cys residues. The first output reported in Figure 8 with chain A of *g*TrxR, showed NBDHEX covalently bound to Cys137 at C4 and C6 (Figure 8A and 8B, respectively), and covalently bound to Cys140 at C4 and C6 (Figure 8C

and 8D, respectively).

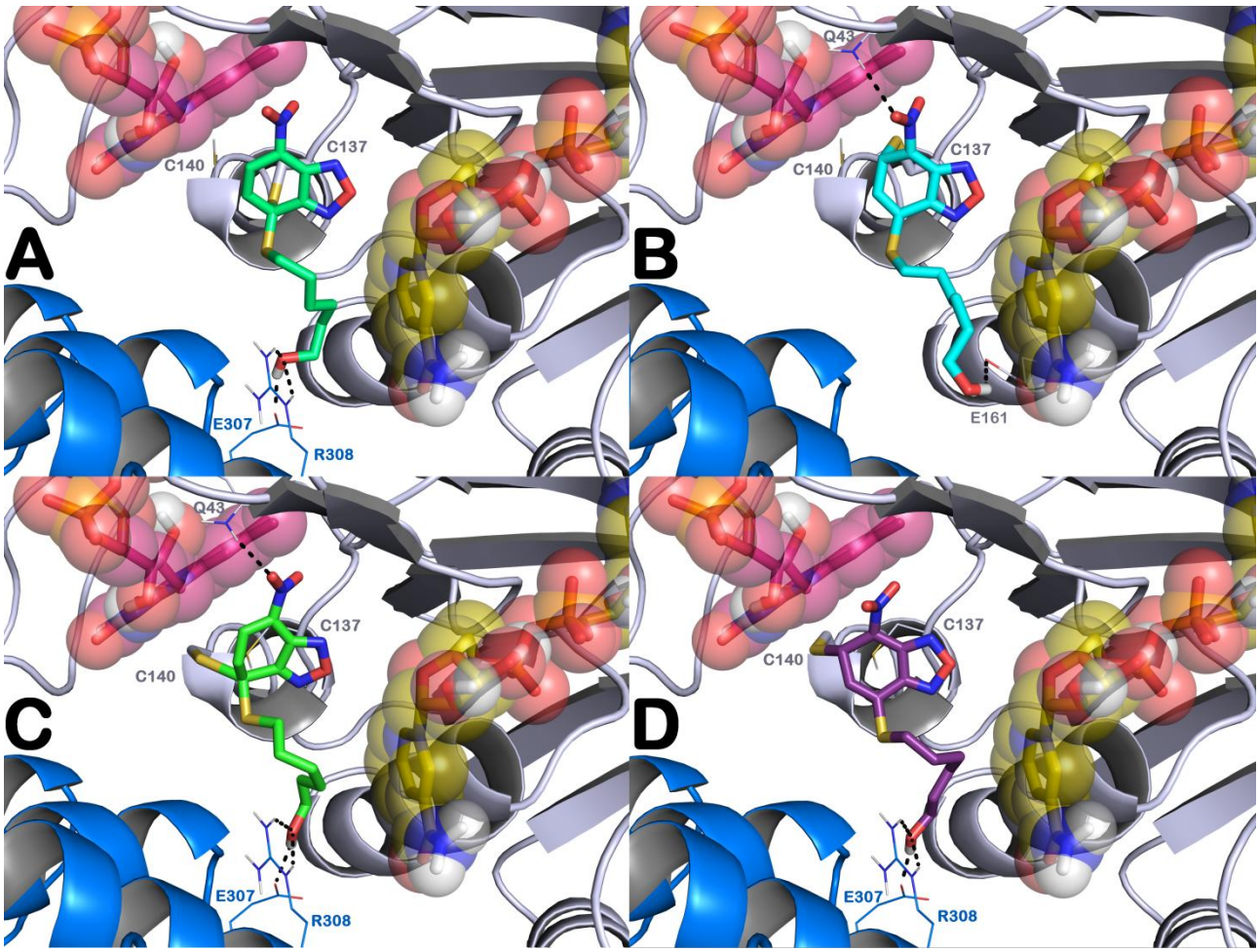

Figure 8. (A,B) NBDHEX (stick) covalently bound to Cys137 (chain A) of monomer A *g*TrxR (grey cartoon) at C4 and C6, respectively. **(C,D)** NBDHEX (stick) covalently bound to Cys140 (chain A) of *g*TrxR (grey cartoon) in position C4 and C6, respectively. Monomer B of gTrxR is represented as blue cartoon, NADPH and FAD cofactors are represented by sticks and spheres in yellow and purple, respectively. H-bonds are represented by black dotted lines. Non-polar hydrogen atoms were omitted for the sake of clarity. The picture was generated by means of PyMOL (The PyMOL Molecular Graphics System, v1.7.2.1; Schrödinger, LLC, New York, 2015).

The analysis of covalent docking calculations, regarding Cys137 at position C4 and C6 showed a slightly different orientation of the thiohexanol chain. In fact, when C4 of NBDHEX is bound at Cys137, it forms a series of H-bonds with residues Glu307 and Arg308 belonging to the chain B (Figure 8A). On the contrary, the covalent bond at C6 with Cys137, H-bonding residue Glu161, pushes the molecule deeper into the binding site precluding its interaction with chain B (Figure 8B).

Regarding the Cys140, NBDHEX is involved in a similar binding mode when the Cys attack occurs at C4 with the unique difference of a further H-bond with Gln43 (Figure 8C). This contact is lost when NBDHEX is bound at C6 (Figure 8D). Moreover, based on the investigation of docking outputs and data we observed a series of interesting information concerning the most accessible cysteine residue: as reported in Table 4, based on docking GlideScore, Cys137 seems easier to be reached than Cys140, forming a more favorable early recognition complex with NBDHEX. When the FAD cofactor is in place, it can physically preclude a more efficient accommodation of NBDHEX, supporting the slight decrease of GlideScore.

The second output, referred to chain B of *g*TrxR, with NBDHEX covalently binding Cys137 at C4 and C6 (Figure 9A and 9B, respectively), and Cys140 at C4 and C6 (Figure 9C and 9D, respectively) is reported in Figure 9. In general, when NBDHEX covalently binds *g*TrxR, due to the conformational change of chain B in AOC, we observed an increase of computational scores in terms of ΔG_{bind} (Table 4) since the ligand can be better accommodated assuming a more favorable conformational energy.

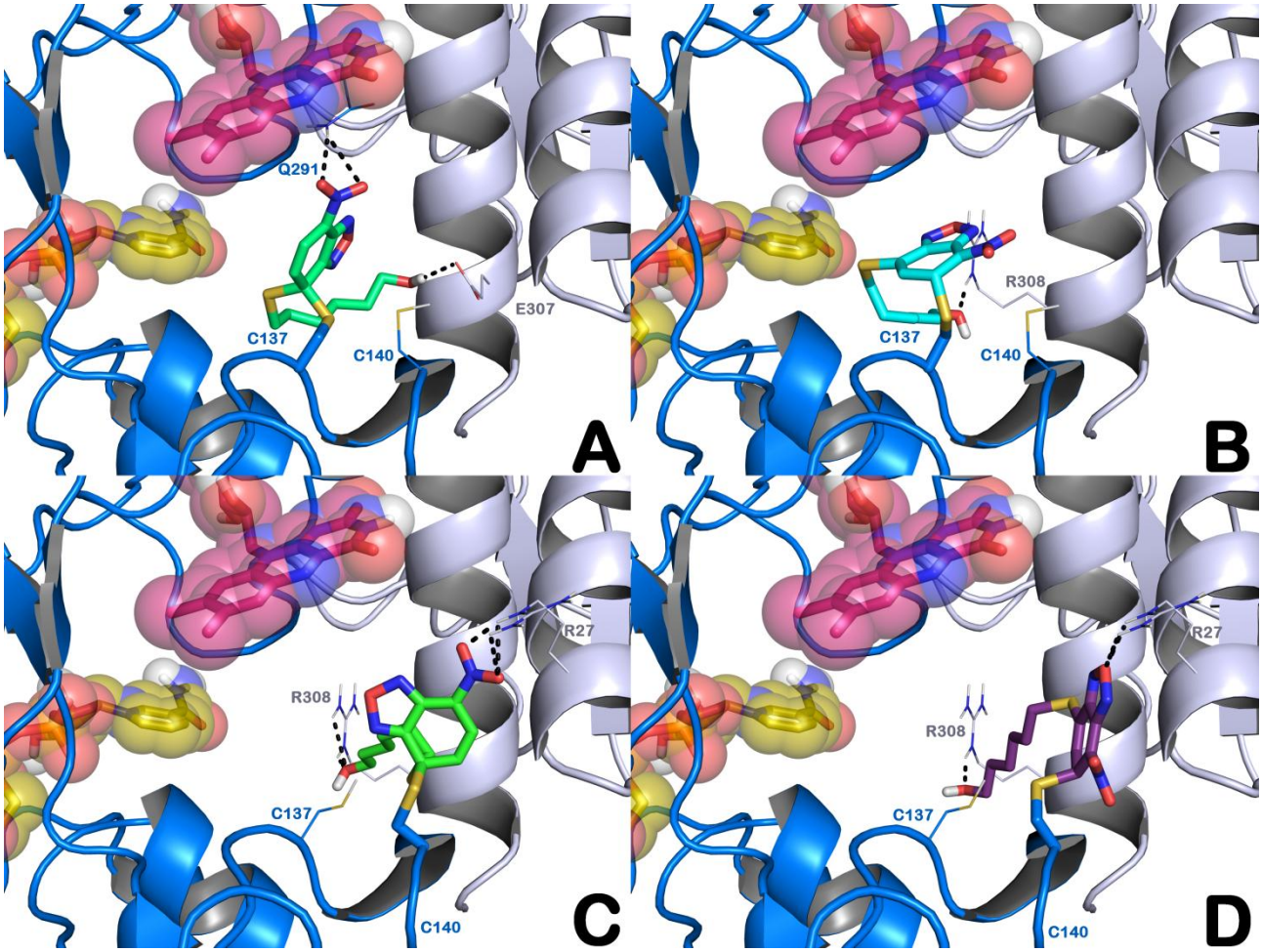

Figure 9. (A,B) NBDHEX (stick) covalently bound to Cys137 (chain B) of monomer B *g*TrxR (blue cartoon) in position C4 and C6, respectively. **(C,D)** NBDHEX (stick) covalently bound to Cys140 (chain B) of *g*TrxR (blue cartoon) in position C4 and C6, respectively. Monomer A of gTrxR is represented as grey cartoon, NADPH and FAD cofactors are represented by sticks and spheres in yellow and purple, respectively. H-bonds are represented by black dotted lines. Non-polar hydrogen atoms were omitted for the sake of clarity. The picture was generated by means of PyMOL (The PyMOL Molecular Graphics System, v1.7.2.1; Schrödinger, LLC, New York, 2015).

The covalent docking calculations for Cys137 bound at C4 and C6 of the ligand (Figure 9A and Figure 9B, respectively) showed a different binding mode denoting different affinities for the mentioned positions as found by the estimation of ligand binding energy (Table A). In fact, also in the AOC the attack of Cys137 to the position C4 results more energetically favorable with respect to the position C6. In particular, NBDHEX when is bound at position C4, H-binds the sidechain of Glu307 belonging to chain A by its thiohexanol chain while with the nitro group is able to form polar contacts with Gln291 belonging to the chain B (Figure 9A). The covalent docking output at position C6 of NBDHEX with Cys137 results in a slight decrease of the number of contacts with only one H-bond with Arg308 (chain A) (Figure 9B).

Regarding the Cys140, NBDHEX is involved in a similar pattern of interaction when the attack occurs at C4 or C6 (Figure 9C and 9D) with the unique difference represented by the orientation of nitrobenzofurazan moiety. In fact, NBDHEX is able to target Arg27 and Arg308 (chain A) with its thiohexanol chain. The nitrobenzofurazan moiety of NBDHEX H-binds the Arg27 residue by the nitro group when it is covalently bound to Cys140 at position C4 (Figure 9C), while H-binds Arg27 by the oxygen from the furazan moiety when it is covalently bound to Cys140 at position C6 (Figure 10D). Due to the enlargement of the binding site in chain B, with respect to the chain A, we observed a similar accessibility to cysteine residues without large differences in docking scores (Table A), deducing that both early recognition complexes are accessible. Remarkably, the analyses of the three best docked poses for each above-mentioned complex (Figures S2-S9) highlighted the

main contacts of NBDHEX into *g*TrxR. In fact, we found that Glu161, Glu307, Arg308 are the key residues governing the NBDHEX interaction with *g*TrxR. Due to the flexible thiohexanol chain, NBDHEX can interact with Glu161 from one chain as well as with Glu307 and Arg308 from the other chain of the enzyme (see Supplementary Material file for further details).

Using the same covalent docking protocol described for NBDHEX we also investigated the binding mode of MTZ covalently bound to *g*TrxR. The reaction between MTZ and the reactive cysteines of the binding site was taken from literature [17] and simulated (see Material and Methods for further details). We observed for MTZ a comparable pattern of interaction with respect to that found for NBDHEX, targeting the same specific residues into the reactive site of *g*TrxR (Figure S10 for the chain A and Figure S11 for the chain B).

The data reported above and the calculated ΔG_{bind} values provide information about the more thermodynamically favored reaction. Although both reactions presented in Figure 7 for NBDHEX could potentially take place, for both monomers, the products obtained from the reaction occurring at C4 of NBDHEX for both cysteine residues are energetically favored with respect to the ones obtained from the reaction occurring at C6. These findings are in perfect agreement with previous data [6, 52, 57]. Our calculations also show that the complexes of NBDHEX with both monomers have comparable binding energies suggesting that both Cys137 and Cys140 could attack NBDHEX at C4 or C6.

3.4. Binding sites analysis and non-covalent docking studies

Based on the experimentally observed biphasic binding of NBDHEX to *g*TrxR and since experimental data could not exclude non-covalent binding of NBDHEX in additional site(s) of the *g*TrxR, distinct from the cysteine-reactive binding site [6], we performed a computational analysis on the entire protein in its dimeric form in order to find potential additional binding sites accessible by NBDHEX. The calculation was performed by SiteMap and the output is reported in Figure 10.

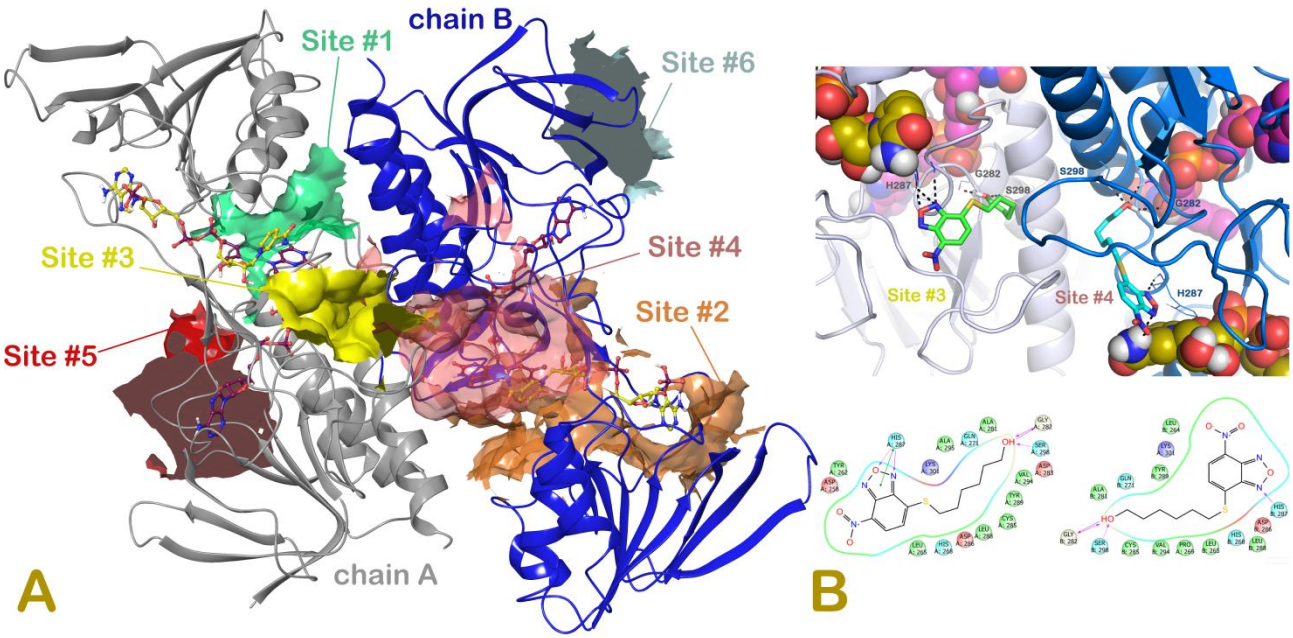

Figure 10. (A) SiteMap output for *g*TrxR (chain A in grey cartoon, chain B in blue cartoon) with highlighted the potential binding sites. NADPH and FAD cofactors are represented by balls and sticks in yellow and purple, respectively. Also disulfide bridges are represented by balls and sticks. The volume of the sites as found by SiteMap is for Site #1 384.07 $Å^3$, for Site #2 659.59 $Å^3$, for Site #3 230.21 $Å^3$, for Site #4 218.14 $Å^3$, for Site #5 52.48 $Å^3$, and for Site #6 83.01 $Å^3$. Sites are ranked by SiteScore as reported by SiteMap. The predicted binding sites Site #1 and Site #2 containing the reactive cysteine residues, corresponding to the binding site of NBDHEX when it is covalently bound to the enzyme. The picture was generated by means of Maestro (Maestro, version 10.1, Schrödinger, LLC, Release 2015). **(B)** Docking output of NBDHEX (sticks) in the additional binding sites Site #3 (chain A; light grey cartoon) and Site #4 (chain B; blue cartoon). NADPH and FAD cofactors are represented by spheres in yellow and purple, respectively. The picture was generated by means of PyMOL (The PyMOL Molecular Graphics System, v1.7.2.1; Schrödinger, LLC, New York, 2015) and ligand-interaction diagram (Maestro. version 10.1, Schrödinger, LLC, Release 2015).

The output revealed a series of potential binding sites suitable for a non-covalent binding of NBDHEX. Despite the conformationally different chains (CC of chain A and AOC of chain B) similar non-covalent binding site were found in both monomers. The calculation was performed

also using the isolated single chains with no difference in the output since the surface of the contacts for protein-protein interactions did not show any cavity that could represent a potential binding site. As expected, we noted only a relevant increase in the volume of Site #2 with respect to its counterpart in the CC Site #1, as well as a slight increase in the volume of Site #6 with respect to its counterpart in the CC Site #5. This is absolutely in line with the large conformational change occurring during the normal dynamics of the enzyme [32]. The results provided by SiteMap highlighted Site #1 (chain A in spring green solid surface in Figure 10A) and Site #2 (chain B in orange solid surface in Figure 10A) as the most accessible sites (cysteines reactions sites above-presented). Among the other sites, Site #3 (chain A in yellow solid surface in Figure 10A) and Site #4 (chain B in pink solid surface in Figure 10A) appears to be probable additional sites for NBDHEX binding, Site #5 (chain A in red solid surface in Figure 10A) and Site #6 (chain B in cyan solid surface in Figure 10A), based on docking calculation, did not present the capability to accommodate NBDHEX due to the poorest computational scores (Table 5).

Table 5. Computational data for the NBDHEX binding different predicted binding sites of both chains of *g*TrxR as found by non-covalent docking protocol.

	Sites					
Computational Scores	**#1 (Chain A)**	**#2 (Chain B)**	**#3 (Chain A)**	**#4 (Chain B)**	**#5 (Chain A)**	**#6 (Chain B)**
GlideScore	-5.97	-4.67	-4.05	-3.49	-1.21	-1.59
ΔG_{bind}	-47.21	-43.11	-37.59	-35.88	-13.17	-15.48

So, the analysis was restricted to the Site #3 and Site #4, and the molecular docking results reported in Figure 10B showed a similar pattern of interaction of NBDHEX into both selected binding sites. In particular, the compound was able to strongly interact with the mentioned binding sites by a series of polar contacts. The thiohexanol chain is able to H-bind Gly282 and Ser298 in both chains. The nitrobenzofurazan moiety is able to form polar contacts with His287 in both chains, while in chain A an additional π-π stacking with His287 was found. Furthermore, a series of hydrophobic contacts with the aliphatic chain of NBDHEX with Leu265 and Pro269 in both chains were

observed, while in chain B additional residues (Tyr289 and Val294) are involved in further hydrophobic contacts. Two polar contacts were found between NBDHEX and NADPH cofactor when the molecule was docked into *g*TrxR chain B. Due to its similar pattern of interaction into both chains the two binding modes of NBDHEX showed comparable docking scores.

4. Conclusion

In summary, we have reported the crystal structure of *g*TrxR in the apo form characterized by the presence of monomers A and B displaying different conformations. While monomer A of *g*TrxR has FO conformation observed for *Sc*TrxR or *Ec*TrxR, monomer B does not adopt the FO conformation but the NADPH binding domain shows a rotation of about -30° with respect to the FAD binding domain, adopting an anticlockwise open conformation where the two catalytic cysteines are far away from the FAD molecule. The different conformations adopted by the two monomers demonstrate that the hinge connecting the two typical Rossman folds (β-α-β-α-β domains) forming the binding sites of NADPH and FAD, respectively, is very flexible and allows the rotation of one domain with respect to the other also in the absence of the substrates. The biological relevance, of the conformation observed in the chain B cannot be argued at the moment.

Other L-TrxRs have been crystallized in the canonical FO CC conformation, in the absence of NADPH [21, 30, 58] but none in the conformation displayed by gTrxR monomer B. However, higher mobility has been observed for the NADPH-binding domain in the absence of the pyridine nucleotide cofactor in the 4CCR structure of *Entamoeba hystolitica* TrxR [21], and the TrxR of barley (PDB code 2WHD) was crystallized without NADPH in an intermediate conformation between FO and FR (with the NADPH and FAD domains rotated to each other of only 49.8°) [30]. Moreover, since the true substrate of gTrxR is still unknown and a canonical thioredoxin seems to be absent in *G. duodenalis* [23], the structural features of *g*TrxR cannot be properly evaluated.

As a final comment, we have shown [6] that, in presence of NADPH, recombinant *g*TrxR can reduces DTNB with a catalytic efficiency of 3.2×10^3 $M^{-1}s^{-1}$, ten times higher than that reported for the TrxR of the closely related enteric parasite *Entamoeba hystolitica* (2.3×10^2 $M^{-1}s^{-1}$) [59]. Thus, it

may be hypothesized a connection between the higher catalytic efficiency of *g*TrxR and the higher flexibility of the NADPH binding domain of *g*TrxR.

These structures were then employed in a comprehensive *in silico* analysis in order to gain some insight into the mechanism governing the inhibitory activity of NBDHEX against the protein. The binding mode of covalently bound NBDHEX was analyzed showing no preferred cysteine residues for covalent reaction. Moreover, we have also identified a reliable accessory binding site for the same ligand that could support the biochemical studies and could be exploited for the identification of novel inhibitors. Except MTZ, none of the drugs currently used against *Giardia* has *g*TrxR as the primary target. In this scenario, NBDHEX is an extremely interesting compound, being activated by *g*TrxR and, at the same time, inhibiting the enzyme itself. Our study paves the way for the rational design of optimized ligands with improved efficacy against *Giardia* infection and sharing the same mechanism of NBDHEX.

Acknowledgments

The authors wish to thank the Helmholtz-Zentrum Berlin (HZB) for the allocation of the Synchrotron radiation beamtime. The British Society for Antimicrobial Chemotherapy (BSAC) is kindly acknowledged (grant number GA2016_087R to SiBr).

Appendix A. Supplementary data

Supplementary data associated with this article can be found in the online version, at…

References

[1] U. Ryan, S.M. Caccio, Zoonotic potential of Giardia, Int J Parasitol, 43 (2013) 943-956.
[2] L. Savioli, H. Smith, A. Thompson, Giardia and Cryptosporidium join the 'Neglected Diseases Initiative', Trends Parasitol, 22 (2006) 203-208.
[3] M. Lalle, Giardiasis in the post genomic era: treatment, drug resistance and novel therapeutic perspectives, Infect Disord Drug Targets, 10 (2010) 283-294.
[4] B.R. Ansell, M.J. McConville, S.Y. Ma'ayeh, M.J. Dagley, R.B. Gasser, S.G. Svard, A.R. Jex, Drug resistance in Giardia duodenalis, Biotechnol Adv, 33 (2015) 888-901.
[5] M. Lalle, S. Camerini, S. Cecchetti, R. Finelli, G. Sferra, J. Muller, G. Ricci, E. Pozio, The FAD-dependent glycerol-3-phosphate dehydrogenase of Giardia duodenalis: an unconventional enzyme that interacts with the g14-3-3 and it is a target of the antitumoral compound NBDHEX,

Front. Microbiol., 6 (2015) 544.
[6] S. Camerini, A. Bocedi, S. Cecchetti, M. Casella, M. Carbo, V. Morea, E. Pozio, G. Ricci, M. Lalle, Proteomic and functional analyses reveal pleiotropic action of the anti-tumoral compound NBDHEX in Giardia duodenalis, Int J Parasitol Drugs Drug Resist, 7 (2017) 147-158.
[7] H.G. Morrison, A.G. McArthur, F.D. Gillin, S.B. Aley, R.D. Adam, G.J. Olsen, A.A. Best, W.Z. Cande, F. Chen, M.J. Cipriano, B.J. Davids, S.C. Dawson, H.G. Elmendorf, A.B. Hehl, M.E. Holder, S.M. Huse, U.U. Kim, E. Lasek-Nesselquist, G. Manning, A. Nigam, J.E. Nixon, D. Palm, N.E. Passamaneck, A. Prabhu, C.I. Reich, D.S. Reiner, J. Samuelson, S.G. Svard, M.L. Sogin, Genomic minimalism in the early diverging intestinal parasite Giardia lamblia, Science (New York, N Y), 317 (2007) 1921-1926.
[8] D.M. Brown, J.A. Upcroft, P. Upcroft, Free radical detoxification in Giardia duodenalis, Mol Biochem Parasitol, 72 (1995) 47-56.
[9] D.M. Brown, J.A. Upcroft, M.R. Edwards, P. Upcroft, Anaerobic bacterial metabolism in the ancient eukaryote Giardia duodenalis, Int J Parasitol, 28 (1998) 149-164.
[10] R.L. Krauth-Siegel, A.E. Leroux, Low-molecular-mass antioxidants in parasites, Antioxid Redox Signal, 17 (2012) 583-607.
[11] M. Muller, Mode of action of metronidazole on anaerobic bacteria and protozoa, Surgery, 93 (1983) 165-171.
[12] D.I. Edwards, Nitroimidazole drugs--action and resistance mechanisms. I. Mechanisms of action, J Antimicrob Chemother, 31 (1993) 9-20.
[13] D. Leitsch, A.G. Burgess, L.A. Dunn, K.G. Krauer, K. Tan, M. Duchene, P. Upcroft, L. Eckmann, J.A. Upcroft, Pyruvate:ferredoxin oxidoreductase and thioredoxin reductase are involved in 5-nitroimidazole activation while flavin metabolism is linked to 5-nitroimidazole resistance in Giardia lamblia, J Antimicrob Chemother, 66 (2011) 1756-1765.
[14] A. Chapman, R. Cammack, D. Linstead, D. Lloyd, The generation of metronidazole radicals in hydrogenosomes isolated from Trichomonas vaginalis, J Gen Microbiol, 131 (1985) 2141-2144.
[15] M. Muller, Reductive activation of nitroimidazoles in anaerobic microorganisms, Biochem Pharmacol, 35 (1986) 37-41.
[16] S.M. Townson, J.A. Upcroft, P. Upcroft, Characterisation and purification of pyruvate:ferredoxin oxidoreductase from Giardia duodenalis, Mol Biochem Parasitol, 79 (1996) 183-193.
[17] D. Leitsch, D. Kolarich, I.B. Wilson, F. Altmann, M. Duchene, Nitroimidazole action in Entamoeba histolytica: a central role for thioredoxin reductase, PLoS Biol, 5 (2007) e211.
[18] D. Leitsch, D. Kolarich, M. Binder, J. Stadlmann, F. Altmann, M. Duchene, Trichomonas vaginalis: metronidazole and other nitroimidazole drugs are reduced by the flavin enzyme thioredoxin reductase and disrupt the cellular redox system. Implications for nitroimidazole toxicity and resistance, Mol Microbiol, 72 (2009) 518-536.
[19] A. Debnath, D. Parsonage, R.M. Andrade, C. He, E.R. Cobo, K. Hirata, S. Chen, G. Garcia-Rivera, E. Orozco, M.B. Martinez, S.S. Gunatilleke, A.M. Barrios, M.R. Arkin, L.B. Poole, J.H. McKerrow, S.L. Reed, A high-throughput drug screen for Entamoeba histolytica identifies a new lead and target, Nat Med, 18 (2012) 956-960.
[20] N. Tejman-Yarden, Y. Miyamoto, D. Leitsch, J. Santini, A. Debnath, J. Gut, J.H. McKerrow, S.L. Reed, L. Eckmann, A reprofiled drug, auranofin, is effective against metronidazole-resistant Giardia lamblia, Antimicrob Agents Chemother, 57 (2013) 2029-2035.
[21] D. Parsonage, F. Sheng, K. Hirata, A. Debnath, J.H. McKerrow, S.L. Reed, R. Abagyan, L.B. Poole, L.M. Podust, X-ray structures of thioredoxin and thioredoxin reductase from Entamoeba histolytica and prevailing hypothesis of the mechanism of Auranofin action, J Struct Biol, 194 (2016) 180-190.
[22] D. Leitsch, Special Issue: Redox Biology of Parasites: Targets for Therapy, Mol Biochem Parasitol, 206 (2016) 1-1.
[23] D. Leitsch, J. Muller, N. Muller, Evaluation of Giardia lamblia thioredoxin reductase as drug activating enzyme and as drug target, Int J Parasitol Drugs Drug Resist, 6 (2016) 148-153.
[24] C.H. Williams, L.D. Arscott, S. Muller, B.W. Lennon, M.L. Ludwig, P.F. Wang, D.M. Veine, K. Becker, R.H. Schirmer, Thioredoxin reductase two modes of catalysis have evolved, Eur J

Biochem, 267 (2000) 6110-6117.
[25] R.P. Hirt, S. Muller, T.M. Embley, G.H. Coombs, The diversity and evolution of thioredoxin reductase: new perspectives, Trends Parasitol, 18 (2002) 302-308.
[26] Z. Faghiri, G. Widmer, A comparison of the Giardia lamblia trophozoite and cyst transcriptome using microarrays, BMC Microbiol, 11 (2011) 91.
[27] G. Waksman, T.S. Krishna, C.H. Williams, Jr., J. Kuriyan, Crystal structure of Escherichia coli thioredoxin reductase refined at 2 A resolution. Implications for a large conformational change during catalysis, J Mol Biol, 236 (1994) 800-816.
[28] B.W. Lennon, C.H. Williams, Jr., M.L. Ludwig, Crystal structure of reduced thioredoxin reductase from Escherichia coli: structural flexibility in the isoalloxazine ring of the flavin adenine dinucleotide cofactor, Protein Sci, 8 (1999) 2366-2379.
[29] T.N. Gustafsson, T. Sandalova, J. Lu, A. Holmgren, G. Schneider, High-resolution structures of oxidized and reduced thioredoxin reductase from Helicobacter pylori, Acta Crystallogr D Biol Crystallogr, 63 (2007) 833-843.
[30] K.G. Kirkensgaard, P. Hagglund, C. Finnie, B. Svensson, A. Henriksen, Structure of Hordeum vulgare NADPH-dependent thioredoxin reductase 2. Unwinding the reaction mechanism, Acta Crystallogr D Biol Crystallogr, 65 (2009) 932-941.
[31] M.A. Oliveira, K.F. Discola, S.V. Alves, F.J. Medrano, B.G. Guimaraes, L.E. Netto, Insights into the specificity of thioredoxin reductase-thioredoxin interactions. A structural and functional investigation of the yeast thioredoxin system, Biochemistry, 49 (2010) 3317-3326.
[32] B.W. Lennon, C.H. Williams, Jr., M.L. Ludwig, Twists in catalysis: alternating conformations of Escherichia coli thioredoxin reductase, Science (New York, N Y), 289 (2000) 1190-1194.
[33] W. Kabsch, Xds, Acta Crystallogr D Biol Crystallogr, 66 (2010) 125-132.
[34] A. Vagin, A. Teplyakov, MOLREP: an automated program for molecular replacement, J Appl Crystallogr, 30 (1997) 1022-1025.
[35] G.N. Murshudov, A.A. Vagin, E.J. Dodson, Refinement of macromolecular structures by the maximum-likelihood method, Acta Crystallogr D Biol Crystallogr, 53 (1997) 240-255.
[36] P. Emsley, K. Cowtan, Coot: model-building tools for molecular graphics, Acta Crystallogr D Biol Crystallogr, 60 (2004) 2126-2132.
[37] R.A. Laskowski, M.W. Macarthur, D.S. Moss, J.M. Thornton, Procheck - a Program to Check the Stereochemical Quality of Protein Structures, J Appl Crystallogr, 26 (1993) 283-291.
[38] S. Butini, M. Brindisi, S. Brogi, S. Maramai, E. Guarino, A. Panico, A. Saxena, V. Chauhan, R. Colombo, L. Verga, E. De Lorenzi, M. Bartolini, V. Andrisano, E. Novellino, G. Campiani, S. Gemma, Multifunctional Cholinesterase and Amyloid Beta Fibrillization Modulators. Synthesis and Biological Investigation, ACS Med Chem Lett, 4 (2013) 1178-1182.
[39] M. Brindisi, S. Butini, S. Franceschini, S. Brogi, F. Trotta, S. Ros, A. Cagnotto, M. Salmona, A. Casagni, M. Andreassi, S. Saponara, B. Gorelli, P. Weikop, J.D. Mikkelsen, J. Scheel-Kruger, K. Sandager-Nielsen, E. Novellino, G. Campiani, S. Gemma, Targeting dopamine D3 and serotonin 5-HT1A and 5-HT2A receptors for developing effective antipsychotics: synthesis, biological characterization, and behavioral studies, J Med Chem, 57 (2014) 9578-9597.
[40] M. Chioua, M. Perez, O.M. Bautista-Aguilera, M. Yanez, M.G. Lopez, A. Romero, R. Cacabelos, R.P. de la Bellacasa, S. Brogi, S. Butini, J.I. Borrell, J. Marco-Contelles, Development of HuperTacrines as non-toxic, cholinesterase inhibitors for the potential treatment of Alzheimer's disease, Mini Rev Med Chem, 15 (2015) 648-658.
[41] M.Y. Wu, G. Esteban, S. Brogi, M. Shionoya, L. Wang, G. Campiani, M. Unzeta, T. Inokuchi, S. Butini, J. Marco-Contelles, Donepezil-like multifunctional agents: Design, synthesis, molecular modeling and biological evaluation, Eur J Med Chem, (2015).
[42] S. Brogi, S. Giovani, M. Brindisi, S. Gemma, E. Novellino, G. Campiani, M.J. Blackman, S. Butini, In silico study of subtilisin-like protease 1 (SUB1) from different Plasmodium species in complex with peptidyl-difluorostatones and characterization of potent pan-SUB1 inhibitors, .J Mol Graph Model, 64 (2016) 121-130.
[43] A. Gasser, S. Brogi, K. Urayama, T. Nishi, H. Kurose, A. Tafi, N. Ribeiro, L. Desaubry, C.G. Nebigil, Discovery and Cardioprotective Effects of the First Non-Peptide Agonists of the G Protein-Coupled Prokineticin Receptor-1, PLoS One, 10 (2015).

[44] S. Giovani, M. Penzo, S. Brogi, M. Brindisi, S. Gemma, E. Novellino, L. Savini, M.J. Blackman, G. Campiani, S. Butini, Rational design of the first difluorostatone-based PfSUB1 inhibitors, Bioorg Med Chem Lett, 24 (2014) 3582-3586.
[45] S. Gemma, S. Brogi, P.R. Patil, S. Giovani, S. Lamponi, A. Cappelli, E. Novellino, A. Brown, M.K. Higgins, K. Mustafa, T. Szestak, A.G. Craig, G. Campiani, S. Butini, M. Brindisi, From (+)-epigallocatechin gallate to a simplified synthetic analogue as a cytoadherence inhibitor for P. falciparum, Rsc Adv, 4 (2014) 4769-4781.
[46] A. Cappelli, M. Manini, S. Valenti, F. Castriconi, G. Giuliani, M. Anzini, S. Brogi, S. Butini, S. Gemma, G. Campiani, G. Giorgi, L. Mennuni, M. Lanza, A. Giordani, G. Caselli, O. Letari, F. Makovec, Synthesis and structure-activity relationship studies in serotonin 5-HT1A receptor agonists based on fused pyrrolidone scaffolds, . Eur J Med Chem, 63 (2013) 85-94.
[47] W.L. Jorgensen, D.S. Maxwell, J. TiradoRives, Development and testing of the OPLS all atom force field on conformational energetics and properties of organic liquids J. Am. Chem. Soc., 118 (1996) 11225-11236.
[48] E. Polak, G. Ribiere, Note sur la convergence de directions conjuguées Rev. Fr. Inform. Rech. Operation., 3e Année, 16 (1969) 35-37.
[49] S.C. Lovell, I.W. Davis, W.B. Arendall, 3rd, P.I. de Bakker, J.M. Word, M.G. Prisant, J.S. Richardson, D.C. Richardson, Structure validation by Calpha geometry: phi,psi and Cbeta deviation, Proteins, 50 (2003) 437-450.
[50] R. Luthy, J.U. Bowie, D. Eisenberg, Assessment of protein models with three-dimensional profiles, Nature, 356 (1992) 83-85.
[51] K. Zhu, K.W. Bonelli, J.R. Greenwood, T. Day, R. Abel, R.S. Farid, E. Harder, Docking Covalent Inhibitors: A Parameter Free Approach To Pose Prediction and Scoring, J Chem Inf Model, 54 (2014) 1932-1940.
[52] M.R. Crampton, L.M. Pearce, L.C. Rabbitt, Kinetic and equilibrium studies of the reactions of 4-nitrobenzofurazan and some derivatives with sulfate ions in water. Evidence for the Boulton-Katritzky rearrangement in a sigma-adduct, J Chem Soc Perk T 2, (2002) 257-261.
[53] S. Giovani, M. Penzo, S. Butini, M. Brindisi, S. Gemma, E. Novellino, G. Campiani, M.J. Blackman, S. Brogi, Plasmodium falciparum subtilisin-like protease 1: discovery of potent difluorostatone-based inhibitors, Rsc Adv, 5 (2015) 22431-22448.
[54] M. Brindisi, S. Gemma, S. Kunjir, L. Di Cerbo, S. Brogi, S. Parapini, S. D'Alessandro, D. Taramelli, A. Habluetzel, S. Tapanelli, S. Lamponi, E. Novellino, G. Campiani, S. Butini, Synthetic spirocyclic endoperoxides: new antimalarial scaffolds, Medchemcomm, 6 (2015) 357-362.
[55] S. Brogi, S. Butini, S. Maramai, R. Colombo, L. Verga, C. Lanni, E. De Lorenzi, S. Lamponi, M. Andreassi, M. Bartolini, V. Andrisano, E. Novellino, G. Campiani, M. Brindisi, S. Gemma, Disease-Modifying Anti-Alzheimer's Drugs: Inhibitors of Human Cholinesterases Interfering with beta-Amyloid Aggregation, CNS Neurosci Ther, 20 (2014) 624-632.
[56] M. Brindisi, S. Brogi, N. Relitti, A. Vallone, S. Butini, S. Gemma, E. Novellino, G. Colotti, G. Angiulli, F. Di Chiaro, A. Fiorillo, A. Ilari, G. Campiani, Structure-based discovery of the first non-covalent inhibitors of Leishmania major tryparedoxin peroxidase by high throughput docking, Sci Rep, 5 (2015).
[57] G. Ricci, F. De Maria, G. Antonini, P. Turella, A. Bullo, L. Stella, G. Filomeni, G. Federici, A.M. Caccuri, 7-nitro-2,1,3-benzoxadiazole derivatives, a new class of suicide inhibitors for glutathione S-transferases - Mechanism of action of potential anticancer drugs, J Biol Chem, 280 (2005) 26397-26405.
[58] J. Obiero, V. Pittet, S.A. Bonderoff, D.A. Sanders, Thioredoxin system from Deinococcus radiodurans, J Bacteriol, 192 (2010) 494-501.
[59] D.G. Arias, E.L. Regner, A.A. Iglesias, S.A. Guerrero, Entamoeba histolytica thioredoxin reductase: molecular and functional characterization of its atypical properties, Biochim Biophys Acta, 1820 (2012) 1859-1866.

Supplementary Material - For Publication Online

Click here to download Supplementary Material - For Publication Online: gTrxR_EJMC_supplementary_final_revised.docx